

SANDIA REPORT

SAND2000-3158

Unlimited Release

Printed January 2001

LDRD Final Report on Designed Ionophores for Liquid-Membrane Separation and Extraction of Metal Ions

John A. Shelnett, Anthony Martino, and James E. Miller

Prepared by
Sandia National Laboratories
Albuquerque, New Mexico 87185 and Livermore, California 94550

Sandia is a multiprogram laboratory operated by Sandia Corporation,
a Lockheed Martin Company, for the United States Department of
Energy under Contract DE-AC04-94AL85000.

Approved for public release; further dissemination unlimited.



Sandia National Laboratories

Issued by Sandia National Laboratories, operated for the United States Department of Energy by Sandia Corporation.

NOTICE: This report was prepared as an account of work sponsored by an agency of the United States Government. Neither the United States Government, nor any agency thereof, nor any of their employees, nor any of their contractors, subcontractors, or their employees, make any warranty, express or implied, or assume any legal liability or responsibility for the accuracy, completeness, or usefulness of any information, apparatus, product, or process disclosed, or represent that its use would not infringe privately owned rights. Reference herein to any specific commercial product, process, or service by trade name, trademark, manufacturer, or otherwise, does not necessarily constitute or imply its endorsement, recommendation, or favoring by the United States Government, any agency thereof, or any of their contractors or subcontractors. The views and opinions expressed herein do not necessarily state or reflect those of the United States Government, any agency thereof, or any of their contractors.

Printed in the United States of America. This report has been reproduced directly from the best available copy.

Available to DOE and DOE contractors from
U.S. Department of Energy
Office of Scientific and Technical Information
P.O. Box 62
Oak Ridge, TN 37831

Telephone: (865)576-8401
Facsimile: (865)576-5728
E-Mail: reports@adonis.osti.gov
Online ordering: <http://www.doe.gov/bridge>

Available to the public from
U.S. Department of Commerce
National Technical Information Service
5285 Port Royal Rd
Springfield, VA 22161

Telephone: (800)553-6847
Facsimile: (703)605-6900
E-Mail: orders@ntis.fedworld.gov
Online order: <http://www.ntis.gov/ordering.htm>



SAND 2000-3158
Unlimited Release
Printed January 2001

LDRD Final Report on Designed Ionophores for Liquid-Membrane Separation and Extraction of Metal Ions

John A. Shelnut
Biomolecular Materials and Interfaces Department

Anthony Martino, James E. Miller
New Materials Theory and Validation Department

Sandia National Laboratories
P. O. Box 5800
Albuquerque, NM 87185-1349

Abstract

New materials and processes for metal-ion separation and extraction based on selective transport of ions across membranes have been developed. Using molecular simulations, porphyrin-based ionophores (molecular ion-carriers) were designed for selectivity in complexing metal ions and other transport properties, such as solubility in organic or aqueous solution. Selectivity was designed into the carriers by controlling basicity, shape, and size of the ionophore specifically for extraction of heavy metals and radionuclides. Promising ionophores were synthesized and tested for application in two different extraction systems. In the first, a supported liquid membrane (SLM) separates two liquid phases--one containing waste and the other a liquid to which the specified metal ions are extracted. The ionophores selectively transport a specified metal ion through the intervening liquid layer to give a pure solution of the metal ion that is easily concentrated. In the second, metal ions were photoreduced to insoluble compounds or elemental metal particles. Separation of the metal particles leaves a pure metal precipitate. These extraction technologies offer convenient new means of separation and extraction for processing Mo-99, decontamination and decommissioning, radioactive waste remediation, and heavy metal waste stream treatment. The initial focus area was on high-level waste tank remediation of heat and gamma emitters (^{137}Cs and ^{90}Sr), long-lived radionuclides (^{99}Tc), and other metal ions contained in high- and low-level waste. Ion-extraction technology with designed ionophores and photoreducers provides increased sustainability and lower cost and complexity of manufacturing processes. Adaptation to pump/treat methods for use at sites such as the White Sands Experimental Test Station and Tuba City were also considered. The technology is differentiated from other efforts (1) by use of molecular simulation to engineer high-performance ionophores and photoreducers, uniting Sandia's chemical, computational, and materials science expertise in a rational, iterative approach, (2) by applying Sandia's recognized expertise in the molecular design of porphyrin-based materials, and (3) by the use of new liquid-membrane and photoreduction technologies.

CONTENTS

	<u>PAGE</u>
I. Introduction	3
II. Results and Discussion	7
III. Conclusions	20
IV. Acknowledgments	20
V. References	21

LDRD Final Report on Designed Ionophores for Liquid-Membrane Separation and Extraction of Metal Ions

Introduction

Industrial and radioactive waste occurs in the form of mixed metal ions and radionuclides in aqueous or organic solutions. Disposal of large volumes of highly radioactive wastes at Hanford, Oak Ridge, Savannah River, and Idaho Falls could benefit from new technologies that lower costs and reduce the volume of waste that must be committed to geologic repositories and minimize secondary waste streams. Specifically, extraction technologies for efficient separation of Tc, Sr, and Cs from tank wastes are priority needs of the ESP-CP, Tanks Focus Area, and Tank Waste Remediation System programs. These new technologies must address current problems including adjustments of the waste stream, addition of materials that adversely impact vitrification, high concentrations of competing ions that reduce separations efficiency, equipment size, and capital costs. These problems justify the development of improved or alternative technologies.

We started with a simple system composed of potassium picrate and potassium chloride as the source phase and water as the receiving phase. The transport rate was followed by the picrate concentration, which is typically the same as the metal ion concentration because charge balance is maintained. The picrate concentration was monitored periodically by its UV absorption by extraction and re-insertion of small samples during the run. The accuracy of the spectrometric method was checked by direct metal concentration measurements.

We have developed efficient and selective technologies for solvent extraction of metal ions through membranes. These membrane solvent-extraction and photoreductive methods are simple and attractive waste treatment approaches, provided by suitable selective ion carriers for transporting the ions across a liquid layer and photocatalysts for reducing metals to an extractable form. Molecular simulation was used to design ion carriers (ionophores) that are highly selective for specified metals. The solubilities of the ionophores were designed so that either aqueous or organic solvents could be used for the membrane, but we concentrated mainly on organic-solvent liquid membranes. Metal-ion transport against a concentration gradient is possible, depending on the different extraction-equilibrium constants at the solvent interfaces and the weak interaction between the carrier and metal salt in the membrane phase. Even more promising and efficient are designed photocatalysts for reducing the metals to particles of insoluble compounds or zero-valent metal. Currently, these extraction processes have been developed for a variety of heavy metals including U, Se, Cr, Mo, Hg, and Pb. These processes involve direct treatment of the wastes and subsequent stripping of the extracted contaminants from the solvent. The ionophore-based methods are similar to the SRTALK process, which uses a crown-ether ionophore in kerosene to remove Tc as pertechnetate ion from alkaline waste. Our approaches differ from standard solvent-extraction-development programs in several ways. The technology is based on new types of ionophores and photocatalysts.

Our membrane approach differs from standard solvent-extraction-development programs in several ways. Firstly, the technology is based on a new type of ionophore that differs radically from the cryptands such as the crown ethers that are currently used. These new ionophores are based on novel nonplanar porphyrins that are being developed at Sandia for a variety of applications. Secondly, the synthesis of the new ionophores was guided by molecular simulation to narrow the search for potentially useful ion carriers. Finally, we integrated the

ionophore development with the development of improved techniques for applying the ionophores to existing waste-treatment problems.

Two alternative ion extraction approaches were pursued--one a supported-liquid-membrane (SLM) technology that avoids direct mixing of the solvent and waste and allows for large-scale continuous-countercurrent flow to permit concentration of the target waste ions in the receiving phase. A second alternative method utilizes a porphyrin-based catalyst or photocatalyst for reducing the soluble metal ions to insoluble particles entrapped in mesoporous silicates to facilitate stripping from the waste stream. This second technique best lends itself to high-value batch-processing applications with demanding specifications like the recovery of ^{99}Mo , but may also be used in a continuous process with occasional replacement of cartridges. The advantages of our approaches over the standard solvent extraction technologies include: potentially greater selectivity, efficiency, reduced solvent and secondary waste generation, and mechanically simple operation. However, our extraction processes retain enough similarity to solvent extraction technologies previously understood and employed in the DOE complex to remain acceptable to process engineers.

Crucial to both technologies is the functional properties of the ion carriers and photocatalysts. Currently known ionophores include crown ethers, calixarene crowns, diaza crown ethers, and ylides. Certain non-planar porphyrins have very recently been suggested as possible ionophores. Others have shown that a *saddled* free base porphyrin selectively binds lithium ions in a 1:1 complex (*1*). In addition, it was reported that Na ions bind 1000 times less effectively. To date, only porphyrins that have a saddled conformation have been found to function as metal ion carriers. The saddle conformation is illustrated in Figure 1. We have varied the conformation and electronic structure of porphyrins to design new efficient and selective ionophores for liquid-membrane ion transport and concentration of toxic metals. Figure 2 shows the complex formed between a technetium(II) ion and one of our novel saddle-shaped porphyrins that was designed for other purposes. Our computational studies indicate that the transport of both positive and negative ion and ion pairs may be possible with analogous porphyrin ionophores.



Figure 1. Saddling and ruffling out-of-plane distortions of porphyrins. The saddle distortion points the lone pair of electrons on the pyrrole nitrogens out-of-plane, allowing them to interact with metal ions. The planar and ruffled porphyrin conformations have the pyrrole nitrogens in the porphyrin mean plane and unavailable for weakly bound metal-ion interactions.

The saddled conformation, in particular, is important in the porphyrin's function as an ion carrier. This deformation from planarity directs the nitrogens of the four pyrrole rings out of the mean plane, allowing them to interact more strongly with metal ions sitting atop the porphyrin macrocycle. This deformation may be necessary for the porphyrins to function as ion carriers.

Based on our initial studies we have used molecular simulations to guide the synthesis of improved ionophores for specified metal ions. The peripheral substituents of porphyrins, which have saddled conformations as the most stable conformation, were altered to vary the magnitude of the saddle deformation and the nature of the cavity in which the metal ion binds. The substituents were also chosen based on their electron-withdrawing/donating properties to control

the basicity (charge) of the pyrrole nitrogens of the porphyrin. In this way, the strength of the interaction of the metal ion with porphyrin was manipulated. For example, in Figure 2 the bromine atoms (brown) withdraw charge at the nitrogens (blue) reducing the interaction with the technetium(II) ion (cyan). The charge on the pyrrole nitrogens is about $+1/3$. We have coupled the computational aspects of the program with experimental measurements of the binding constants and ion selectivities. In this manner, we have identified the molecular parameters affecting performance, *e.g.*, charge density, conformational distortions, basicity etc., and verified our computational models.

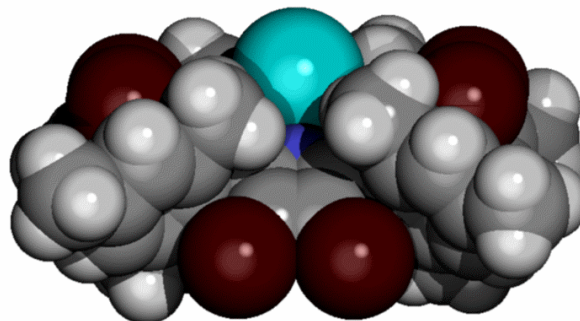


Figure 2. Free base octobromo-meso-tetramesitylporphyrin with technetium(II) ion electrostatically bound.

More than ten free-base porphyrin ionophores were synthesized and evaluated for their ion-transport properties. Both supported-liquid membranes and bulk-liquid membranes were used in the transport testing protocols. The ionophores included some porphyrins that are highly non-planar and therefore expected to be good carriers. The ionophores tested exhibited a wide range of ion-transfer rates, varying from almost no transport to some which are comparable to or better than currently used ion carriers. As expected, the planar porphyrins are poor carriers, consistent with our initial hypothesis and also our molecular simulations of the porphyrin-ion complexes. We suspected that out-of-plane saddling of the porphyrin would be necessary in order to expose the lone pairs on the nitrogens so that they could interact more effectively with the ion. The perceived requirement for saddling of the porphyrin structure turned out to be not so important however. The reason is that many free-base porphyrins are highly flexible and thus easily become saddled due to H-bonding, van der Waals, and ionic interactions with the porphyrin core. This unexpected outcome effectively broadens the base of possible porphyrins suitable for computer design and synthesis as new ionophores. Most interesting is a novel tetrameric calix[4]arene-porphyrin ionophore. Many of the designed and synthesized ionophores have been structurally characterized with UV-visible absorption, NMR, X-ray crystallography, and resonance Raman spectroscopy. Most useful were the X-ray crystal structures of dodecaphenylporphyrin-picric acid complexes and the calix-arene porphyrin. We also attempted to use ^7Li NMR to investigate Li^+ -ionophore complexes. Relationships between porphyrin conformational and electronic properties and their ion-transport rates were found and this information was incorporated into the molecular design procedures. For example, the presence of electron-withdrawing substituents on the porphyrin increases ion-transport rates and is thus desirable.

Several examples of a new type of porphyrin-based ionophore that can act as the negative organic counter-ion were synthesized and evaluated for their ion-transport properties. These ionophores represent a potentially significant advance in the technology because they hold up the possibility of eliminating the addition of an organic counter-ion, a requirement common with most existing ionophores. Bulk-liquid membranes were used in the transport testing protocols. Metal ion complexes with the new ionophores were identified by spectroscopic methods. The new ionophores allow metal ions in the source to be exchanged for protons in the receiving phase. The possibility exists for extraction of very low-level contaminants by forced extraction using a pH gradient.

We discovered a promising new *in-situ* reductive treatment of uranium mine tailings, which potentially utilizes only the environmentally benign reactants hydrogen and the naturally occurring proteins, hydrogenase and cytochrome c_3 . With Prof. Werner Lutze at UNM, we found that this metal-reduction method is suitable for use in a “wagon wheel” treatment system, which Prof Lutze used previously for microbial treatment of nitrate contaminated sites. The method utilizes the ability of the proteins such as cytochrome c_3 to reduce U^{+6} to U^{+2} , which then slowly precipitates as the mineral uraninite. The process thus lowers the solubility to EPA acceptable limits, providing a long-term solution to the problem. The method is environmentally benign since only proteins from naturally occurring nitrate and sulfate-reducing bacteria are utilized along with H_2 for regenerating the reduced cytochrome c_3 . A version of this novel new approach may also be used to extract plutonium from sites where the contamination is above the ground-water saturation zone.

We subsequently found that this cytochrome c_3 method could also be used for many other heavy metal contaminants including Cr, Mo, Hg, Pb, Se, Cu, Ag, Pt, and Au. Cytochromes c_3 contain four iron-porphyrins, which act as electron-transfer catalysts. A strong reductant such as the H_2 /hydrogenase system or an inorganic chemical reductant provides the electrons required to reduce the metal salts to insoluble forms.

Finally, we developed a Sn-porphyrin-based photochemical system for producing the strong reductant needed to reduce most of the metals listed above. The photoexcited Sn porphyrin is reduced by a variety of environmentally benign weak electron donors to give a strongly reducing porphyrin radical anion that is capable of photocatalytically reducing many metal salts to insoluble forms—zero-valent metal particles in most cases. This biomimetic photochemical process is suitable for treating metal-contaminated water in a solar reactor via a continuous-flow pump and treat process. It has an advantage over other photocatalysts such as TiO_2 in that it utilizes the entire UV and visible portions of the solar spectrum. These reductive ion extraction methods are much more efficient than the liquid membrane methods and are to be preferred for most applications.

Results and Discussion

Testing procedures for liquid membranes and reductive extraction. The ion extraction approach developed utilizes a supported-liquid-membrane (SLM) technology that avoids direct mixing of the solvent and waste and potentially allows for large-scale continuous-countercurrent flow to permit concentration of the target waste ions in the receiving phase. A second alternative method utilizes direct reduction and precipitation of metal waste followed by stripping. This second technique may ultimately best lend itself to high-value batch-processing applications with demanding specifications like the recovery of ^{99}Mo . The advantages of our approach over the standard solvent extraction technologies include greater selectivity, efficiency, reduced solvent and secondary waste generation, and mechanically simple operation. These extraction processes retain enough similarity to solvent extraction technologies previously understood and employed in the DOE complex to remain acceptable to process engineers.

Two types of ion-transport testing procedures have been developed and used to evaluate the porphyrin ionophores. For the first, the testing cell is illustrated in Fig. 1. We are using this simple apparatus to measure ion transport across a bulk liquid membrane. The cylindrical cell containing an organic solvent (typically, dichloromethane) at the bottom serves as the organic-solvent membrane phase into which the ionophore is added. A concentric glass tube is introduced into the organic solvent and the aqueous source phase containing the target ions to be extracted is carefully added into the outer ring and floats on top of the organic phase. The aqueous receiving phase is then introduced into the inner cylinder. The organic-solvent phase is magnetically stirred during the reaction. Ions are transported from the source into the receiving phase through the organic solvent and monitored by the ion concentrations, followed by UV-visible absorption spectroscopy. Typical rate data are shown in Fig. 2; the data points are averages of five independent measurements.

A second device (not shown) with two chambers separated by a porous material (Celgard 2400-isotatic polypropylene) containing an organic solvent, typically toluene, was also used, and ion transfer was followed by conductivity measurements. In the SLM process, ion transfer was followed by conductivity measurements, and typically shows a linear increase in conductivity as ions are transferred across the supported liquid membrane. The conductivity typically shows a 1-hour induction period followed by a linear increase in conductivity as ions are transferred across the supported liquid membrane.

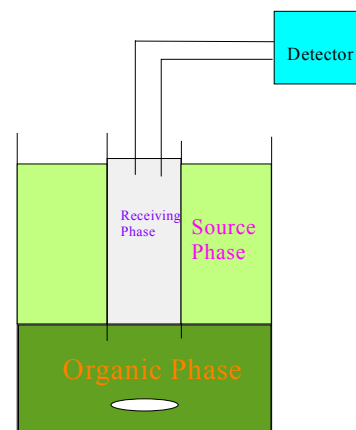


Fig. 1. Ion-transport cell for screening transport activity of porphyrin ionophores.

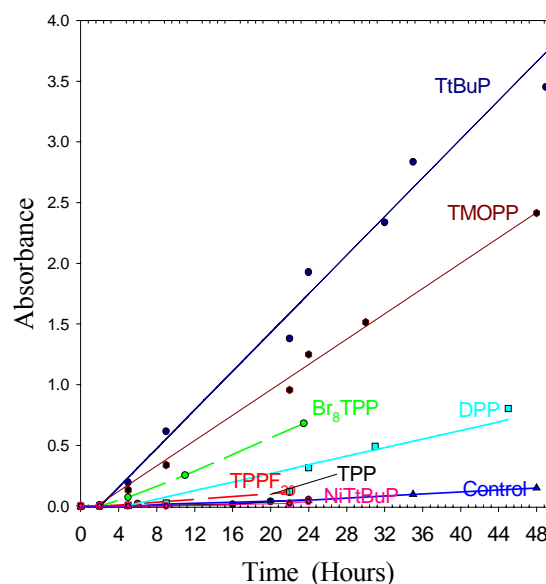


Fig. 2. Ion-transfer rates for different porphyrins as measured by the absorbance of picrate ion in the receiving phase.

Evaluation of non-planar porphyrins as ion carriers. We have screened many free-base porphyrins of differing conformations to determine whether only the saddled conformers are capable of transporting metal ions. We have also determined some other relationships between structure and ion-transport activity from the rate data shown in Fig. 2. These studies have determined the protocols for our experimental measurements of ion-transport properties. In some cases (*e.g.*, the data in Fig. 2), we have used Tris buffer in the aqueous source and receiving phase to control the pH. The source phase initially contains metal chloride (0.1 M) and picrate metal salt (0.001 M).

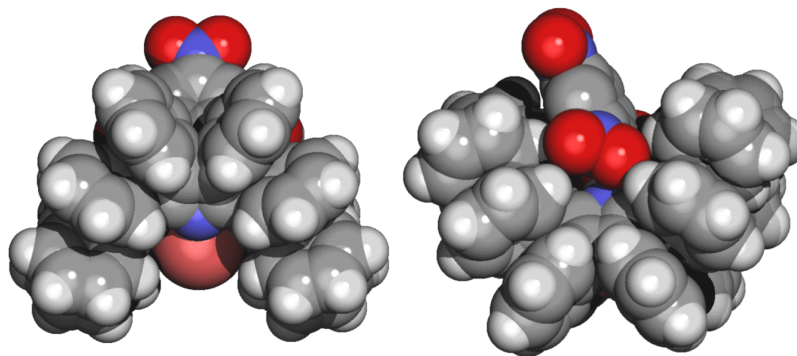


Fig. 3. Molecular simulation of Na^+ (pink) complexed with dodeca-phenyl porphyrin free base. Picrate serves as the counter ion for transport across an organic liquid membrane.

Crucial to both membrane technologies is the functional properties of the ion carrier. Currently known ionophores include crown ethers, calixarene crowns, diaza crown ethers, and ylides. Certain non-planar porphyrins have recently been suggested as possible ionophores, including a saddled free base porphyrin that selectively binds lithium ions in a 1:1 complex and that exhibits selectivity factor of 1000 relative to Na). Building on this result, we have shown that such porphyrin-ion complexes also function as efficient ion carriers. We have also shown that the molecular structure of the ionophore is an essential parameter in determining ion transport. In particular, it was initially thought that only porphyrins with a saddled conformation would act as efficient ionophores, but we have now found that other nonplanar conformations are just as or more effective than the saddled conformer. The saddle conformer for the dodecaphenylporphyrin-picrate-metal-ion complex is illustrated in Fig. 3. We chose porphyrins that vary the conformation and electronic structure, and concomitantly, the efficiency and selectivity when acting as an ionophore. Indeed, the porphyrins are seen (Fig. 2) to vary significantly in their ion-transport properties, from virtually no activity for planar porphyrins to ion-transport efficiencies similar to currently known ionophores like the crown ethers.

We subsequently discovered that transport across the organic liquid membrane (dark green) in Fig. 1 involves both proton transport as well as metal ion transport for the ionophores we have employed so far. This discovery has had two main consequences for the direction of our development of

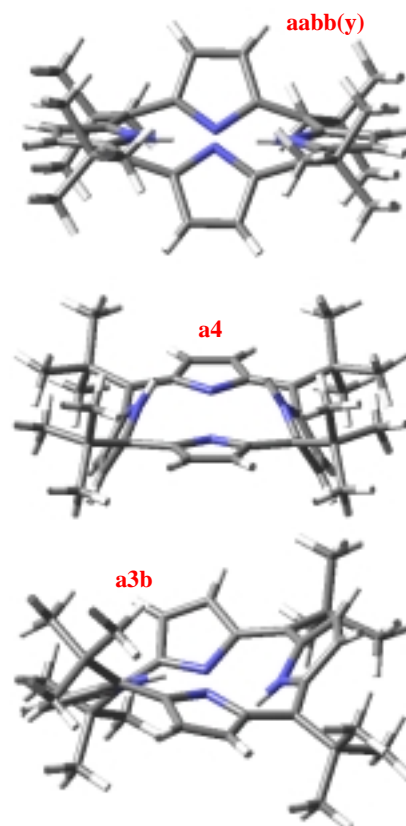


Fig. 4. H_2TtBuP conformers show that a porphyrin that is purely ruffled as a metal porphyrin has its nitrogens directed out-of-plane for the free-base-porphyrin analog.

this class of ionophores. First, the molecular design goals were altered to design more efficient and selective ionophores of this type, and to accomplish this we needed a more complete understanding of the interaction of metal ions with the ionophores. To obtain this new information, X-ray crystal structures of the ion-ionophore complexes were obtained (Fig. 7). Second, for a field-deployable waste treatment method, picric acid, which is an explosive when dry, should to be eliminated from the process. Thus, using the ionophore itself instead of picrate as the counter-ion for the metal became a more important goal, focusing our efforts more on the fundamental processes involved in the metal ion-ionophore complex.

By screening the transport properties of many porphyrin ionophores, we have determined that the structure of the porphyrin has a large effect on ion-transport. Moreover, we also found that proton-transport competes with the desired metal-ion transport. Our hope was to capitalize on this discovery in two ways—first, by formulating new ionophores that function by a new mechanism based on the proton-transport properties to actively pump metal ions across a membrane and, second, by designing new ionophores of the picrate-salt type that are metal-ion selective and less susceptible to proton leakage.

Computer-design and synthesis of new ionophores. Fig. 3 shows the calculated complex postulated to be formed between sodium picrate and one of our novel saddle-shaped porphyrins. This type of complex has not been seen before. Our computational studies indicate that the transport of both positive and negative ion and ion pairs is feasible with analogous porphyrin ionophore complexes. The saddled conformation, in particular, was thought to be important in the function of porphyrins as ion carriers simply because this out-of-plane distortion directs the nitrogens of the four pyrroles out of the mean plane so that they are available to interact with ions sitting atop the porphyrin macrocycle. However, we found that this distortion does not necessarily have to be built into the porphyrin for it to function as an ion carrier. By comparing the transport properties of planar, ruffled, and saddled porphyrins with similar electronic properties, we have found that the free base porphyrins are amazingly flexible, allowing them to adopt a variety of

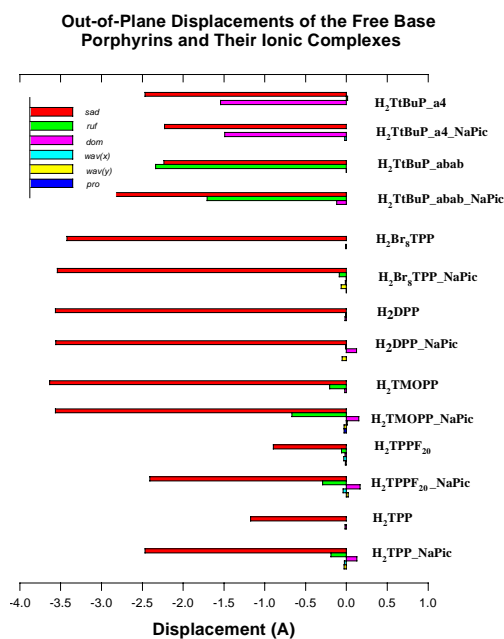


Fig. 5. Out-of-plane displacements along the lowest-frequency normal coordinates of each symmetry type for conformers of porphyrin ionophores and their Na complexes.

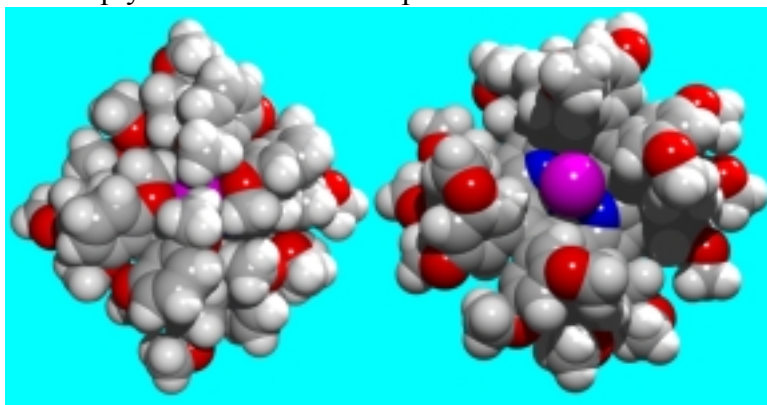


Fig. 6. Molecular simulations of Na^+ (magenta) complexed with free base tetra-*p*-methoxyphenyl- β octa(*o*/*m*-dimethoxyphenyl)porphyrin derivatives: ortho (left) and meta (right). The *o*-methoxy groups severely crowd K^+ , but not Na^+ and Li^+ ions. The methoxy groups also increase ion solubility in the organic phase.

geometries that can transport ions. For example, Fig. 4 shows three of the stable structures of free base tetra-tert-butylporphyrin (H_2TtBuP), a porphyrin that was expected to be ruffled, not saddled, based on earlier calculations for its metal derivatives. We find that of the three lowest energy conformers none is purely ruffled and all have nitrogens lone pairs or hydrogens directed out of the mean plane of the molecule, *i.e.*, a substantial saddling component to the nonplanar distortion.

One deficiency in most porphyrins when used as ionophores is the relative non-polar substituent groups surrounding the metal binding site. Thus, we designed several new porphyrins to increase the polarity of the metal site to increase metal uptake. An example is the porphyrin (DPP) shown in Fig. 6, which has been modified to include 20 methoxy substituents in the *ortho* and *meta* positions of the phenyl substituents, greatly increasing the polarity of the metal binding site. These porphyrins have been designed to operate by the original metal ion-transport mechanism using picrate as the counter-ion. The incorporation of many methoxy groups near the binding site increases metal-ion binding affinity and solubility in the organic phase. The methoxy groups act much like a crown-ether ionophore, increasing the metal-ion solubility in the organic phase and thus the transfer efficiency. In addition, the methoxy groups help increase the porphyrin solubility, further increasing transfer rates. The different positions (*meta* and *ortho*) of the methoxy groups on the phenyl substituents for the two $H_2DPP(OMe)_{20}$ derivatives give radically different ion-size selectivity for the metal binding site. For example, the binding energy for K^+ is calculated to be $4 \text{ kcal}\cdot\text{mol}^{-1}$ higher than for Na^+ , for the *ortho* derivative, but less than $1 \text{ kcal}\cdot\text{mol}^{-1}$ higher, for the *meta* derivative. This is expected to provide selectivity in ion transport. The *meta*-OMe derivative has been synthesized.

Other porphyrin ionophores were designed based on the structure-activity relationships that have been discovered (see below).

Structural characterization of new ion carriers. NMR, resonance Raman and UV-visible absorption spectroscopy have been used to structurally characterized the new porphyrins, as well as the ionophore-ion complexes. This work is exhaustively considered in recent publications (2-39). We have also carried out normal-coordinate structural decomposition (NSD), a Sandia developed technique, on some of the X-ray crystal structure and also the calculated structure like those shown in Figure 4. The NSD results are shown in Figure 5 for some of the calculated structures of the ionophore-ion complexes. An increase in the saddling contribution to the structure is clearly evident upon ion binding in these complexes for the less saddled conformers.

Fig. 7 shows the X-ray crystal structure of the porphyrin-picric acid complex that mediates the proton leakage process. Out of about 10,000 known porphyrin crystal structures, this represents the first complex of this type. The crystallization of this complex has greatly improved our understanding of the ion-transport properties. In addition, comparing with the calculated structure of the sodium picrate complex with dodecaphenylporphyrin (Fig. 3) demonstrates the high accuracy of the computer modeling. However, modeling alone cannot say what type ion complexes are actually formed under the ion-transport conditions. This complex

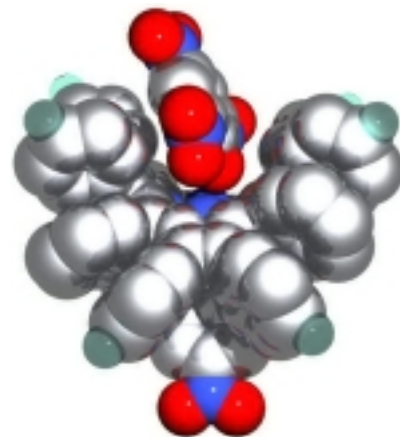


Fig. 7. X-Ray crystal structure of the bis-picric acid complex with free-base dodecaphenylporphyrin- F_8 . The hydrogen atoms not shown.

mediates the transport of picrate anion and protons, but not metal ions, across the membrane. Fortunately, maintaining a 2-pH-unit difference between the source and receiving phases can shut down this proton-leakage process. Under these conditions, the picrate concentration in the receiving phase is an accurate measure of the metal ions transported across the membrane; however, we find that the transfer rate is significantly less than anticipated. New porphyrin ion carriers that take the proton-leakage problem into account could now be designed and synthesized.

$\text{H}_2\text{Br}_8\text{T}(\text{CF}_3)\text{P}$ and $\text{H}_2\text{T}(\text{CF}_3)\text{P}$ are two newly designed and synthesized porphyrin ionophores of this type. X-Ray crystal structures of these ionophores have been obtained for their Ni derivatives and that of $\text{NiBr}_8\text{T}(\text{CF}_3)\text{P}$ is shown in Fig. 8. Ion-ionophore complexes formed are described in the next section.

Fig. 9 illustrates another new type of ionophore that incorporates both porphyrins and traditional calix[4]arene ionophores—similar to calix[4]arene-crowns that have been used in ion-transport systems for cesium and silver ions. The crystal structure of this calix[4]arene-porphyrin (Fig. 9) has been solved.

An interesting feature of the porphyrin system H_2P is its unusual protonation behavior compared to other dibasic systems. For example, optical studies reveal strikingly low concentrations of the intermediate monocation H_3P^+ when porphyrins are titrated with strong acids to produce the dication H_4P^{2+} , especially in the case of 5,10,15,20-tetraarylporphyrins such as H_2TPP . In addition, ^1H NMR studies show that the activation energy for free base-dication proton exchange in H_2TPP is unexpectedly high compared to β -octaalkylporphyrins. While the origins of these anomalies are not fully understood, it has been speculated that they are related to the saddle deformations that are known to occur when the porphyrin ring is protonated. Given the current interest in the synthesis and properties of nonplanar porphyrins, we decided to investigate the protonation of H_2OETPP and $\text{H}_2\text{T}(\text{tBu})\text{P}$, two conformationally designed porphyrins which adopt very saddled or ruffled conformations. These studies provide answers to longstanding questions about the atypical protonation behavior of porphyrins, and also allow the first detailed ^1H NMR characterization of a true porphyrin monocation. The NMR spectrum is given in Fig. 10.

Coincidentally, our investigation of the metal-ion transport behavior of nonplanar porphyrins using picrate as the anion also helped us to answer some longstanding questions regarding the unusual protonation behavior of porphyrins. It is well established that optical spectra taken during the titration of porphyrins with strong acids reveal strikingly low concentrations of the intermediate monocation H_3P^+ compared to the final dication product H_4P^{2+} , especially in the case of 5,10,15,20-tetraarylporphyrins such as H_2TPP .^{1,2} In addition, ^1H NMR studies show that the activation energy for free base-dication

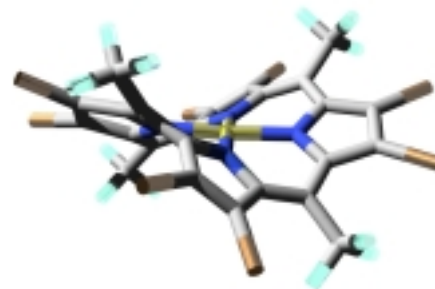


Fig. 8. X-Ray crystal structure of $\text{NiBr}_8\text{T}(\text{CF}_3)\text{P}$, a new type of ionophore.

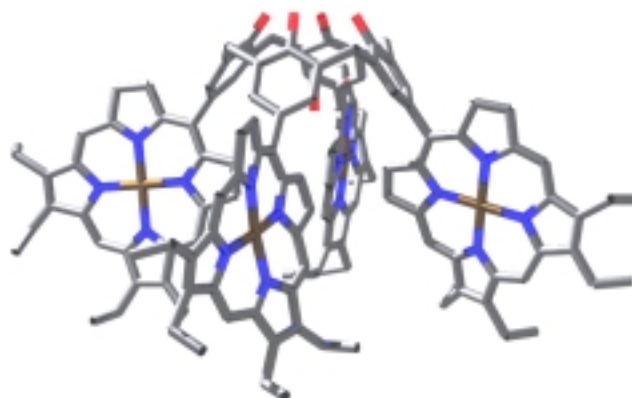


Fig. 9. X-Ray crystal structure of a calix[4]arene-porphyrin nickel derivative—a new type of ionophore. New ionophores will be designed based on this type of structure.

proton exchange in H_2TPP is unexpectedly high compared to β -octaalkylporphyrins. While the origins of these anomalies are not fully understood, it has been speculated that they are related to the saddle deformations that are known to occur when the porphyrin ring is protonated. Given the current interest in the synthesis and properties of nonplanar porphyrins, we decided to investigate the protonation of H_2OETPP and $H_2T(tBu)P$, two conformationally designed porphyrins which adopt very saddled or ruffled conformations. These studies allowed essentially a complete understanding of how protonation-induced conformational changes lead to the atypical protonation behavior observed in the case of porphyrins. The first detailed 1H NMR characterization of a true porphyrin monocation was also possible because the elusive monocation was formed in large amounts by H_2OETPP in the presence of picric acid (Fig. 10).

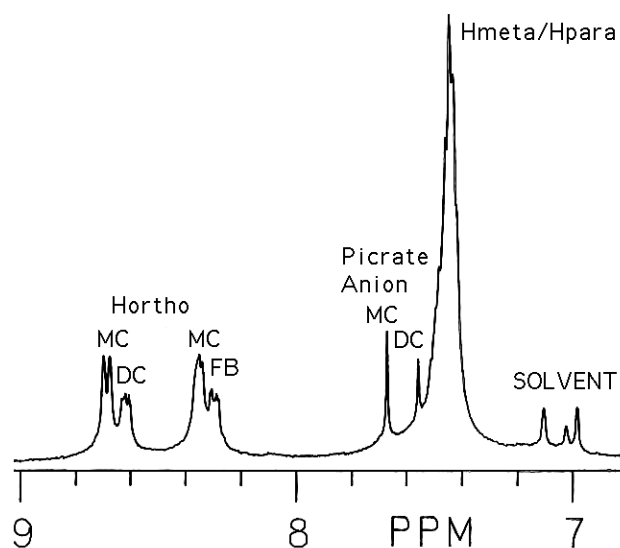


Fig. 10. Aromatic region of the 300 MHz 1H NMR spectrum of H_2OETPP in toluene- d_8 containing picric acid (FB= free base, MC = monocation, DC = dication).

Structure-activity relationships. The substituents have also been chosen based on their electron-withdrawing/donating properties, which we have found to control the basicity (charge) of the pyrrole nitrogens of the porphyrin. Our studies show that the strength of the interaction of the ions with porphyrin can be manipulated to some extent in this way. For example, in Fig. 2 the eight bromine atoms of Br_8TPP are seen to increase the ion-transfer rate (slope) relative to TPP , although this could result from the near planarity of TPP . However, comparison of the rates for DPP and $F_{20}DPP$ show the same trend, and, in this case, there is no difference in conformation. Thus, it appears that electron-withdrawing substituents are desirable, and, consequently, several new porphyrins including $T(CF_3)Br_8P$ have been designed and synthesized. Further improvements in the ionophore design could still be made based on how other molecular parameters affect ion-transport performance.

Metal-ion transport selectivity. 7Li NMR provides an additional method for accurately determining the metal-ion transfer rates independently of the rates for protons or organic anions. For example, 7Li NMR has been extensively investigated as a means of directly detecting Li^+ concentrations. We have used 7Li NMR to investigate Li^+ -ionophore complexes for determining selectivity and the nature of the ion-ionophore complex.

For the porphyrin ionophores that can function as the organic counter-ion, we need a nonplanar porphyrin

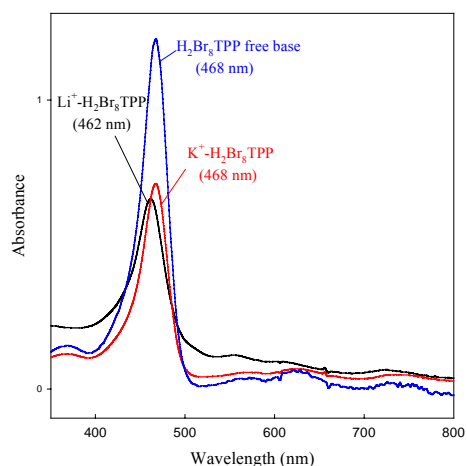


Fig. 11. UV-visible absorption spectra of metal-ion complexes with H_2Br_8TPP .

with electron-withdrawing substituents such as the related water-soluble porphyrin, $\text{H}_2\text{Br}_8\text{T}(\text{N-MePy})\text{P}$, which is known to selectively bind Li^+ in a 1:1 complex with a selectivity factor of 1000 relative to Na^+ (1). However, to be an efficient and selective ion carrier the porphyrin should be soluble in organic solvents. $\text{H}_2\text{Br}_8\text{TPP}$ is soluble in organic solvents and has previously been shown to work by the conventional transport mechanism, although it primarily transports protons rather than metal ions. The difference here is that the pH of the source and receiving aqueous phases is adjusted so that at the high pH source phase, the porphyrin loses a proton and gains a negative charge so that it supports the binding and solubilization of a metal ion. At the neutral-pH-receiving phase, the metal ion is released from the neutral ion-ionophore complex and a proton is then delivered back to the high-pH-source phase. That is, protons flow in one direction and metal ions flow in the other.

Selectivity has been demonstrated by the UV-visible absorption spectra of the complexes of K^+ , Li^+ , and H^+ with HBr_8TPP^- shown in Fig. 11. The K^+ and Li^+ complexes are formed in the organic phase during the ion-transport measurement when the source phase contains either 0.1 N KOH or LiOH, respectively. The smaller Li^+ ion has a larger influence on the spectrum causing a 6-nm blue shift in the porphyrin Soret absorption band. The much larger K^+ ion causes no shift in the Soret band relative to $\text{H}_2\text{Br}_8\text{TPP}$, but the relative intensities of the weak absorption bands between 500 and 800 nm do change. The solubility of the K^+ complex is much less than for Li^+ since a precipitate forms in the organic phase for K^+ . K^+ is not efficiently transported to the receiving phase because of the poor solubility in CH_2Cl_2 . Other liquid-membrane solvents may increase solubility, and the porphyrin can also be modified to increase solubility of the complex and improve transport rates. Ion-transport properties of porphyrins are known to vary with structure, and undoubtedly, this will be the case for this new transport mechanism.

Photoreductive-Precipitation Extraction Methods. Biological processes for removing heavy metals from wastewater include biosorption, bioaccumulation and bioreduction. However, these processes can fail to lower the concentrations of metals below regulatory standards due to toxicity to living microorganisms or rapid saturation of adsorbing sites of biomass. Using proteins such as cytochrome c_3 eliminate these limitations. Cytochrome c_3 exhibits selective and high-affinity binding sites for electron transfer and catalyze redox reactions in solution.

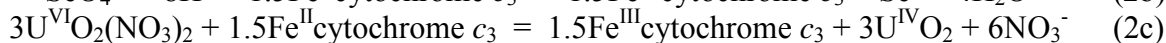
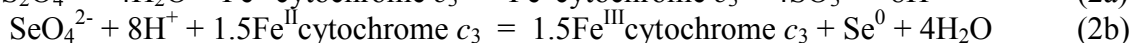
An innovative way to develop effective and environmentally benign processes for water treatment involves the use of specific enzymes extracted from microorganisms. Lovley et al. (1993) and Lovley and Phillips (1994) showed that cytochrome c_3 , purified from *Desulfovibrio vulgaris*, can be used to separate dissolved uranium and chromium species from water by reduction and precipitation of sparingly soluble compounds of these metals. More recently, Lojou et al. (1998) and Lojou and Bianco (1999) showed that several c-type cytochromes including cytochrome c_7 from *Desulfovibrio acetoxidans*, cytochrome c_3 from *D. vulgaris* Hildenborough, *D. desulfuricans* Norway, *D. gigas*, and cytochrome c_{553} from *D. vulgaris* Hildenborough reduce soluble Fe(III), Cr(VI), U(VI) and oxides of Mn(IV), V(V) and Fe(III). The tetraheme protein cytochrome c_3 , first identified in sulfate-reducing bacteria, is responsible for the reduction of elemental sulfur to sulfide by these bacteria. Cytochrome c_3 was also found in the facultative anaerobic bacterium *Shewanella putrefaciens*. Chapman et al. (1997) described this four heme protein as “the most versatile redox center in biology”. Biocatalysts (*e.g.*, enzymes) are the ideal “green” catalyst for redox reactions, producing less waste and consuming less energy. Using cytochrome c_3 rather than living cells of sulfate-reducing bacteria eliminates their intoxication and loss of effectiveness caused by high concentrations of contaminants. Also,

reduction of metals by cytochrome c_3 has been shown to be very fast. The redox potential of the hemes of cytochrome c_3 can be as low as $E_H \approx -400$ mV, a value low enough to reduce all higher valence states of metals. If not reduced to the metallic state, many metals form insoluble oxides or hydroxides in lower valence states.

The center of each heme molecule in cytochrome c_3 consists of an iron atom. The iron atom changes valence between Fe(II) and Fe(III) during electron transfer. The reaction between the cytochrome c_3 and a given bivalent cation (M^{2+}) can be described by the following reaction:



assuming the electron of all four hemes is transferred. Cytochrome c_3 can also be reduced electrochemically on platinum, mercury, and carbon electrodes or chemically, *e.g.* by sodium dithionite. The catalytic role of cytochrome c_3 can be expressed by reactions (2a-d):



Reaction (2b) shows reduction to the zero-valence state [$\text{Se}(\text{VI}) \rightarrow \text{Se}^0$]; reaction (2c) reduction to a lower valence state [$\text{U}(\text{VI}) \rightarrow \text{U}(\text{IV})$] and formation of sparingly soluble UO_2 ; reaction (2d) shows reduction of dissolved oxygen. All reactions are mediated by cytochrome c_3 . Direct reduction of most metal ions by dithionite is thermodynamically possible but the reactions are too slow to be of practical interest. Cytochrome efficiently catalyzes these reactions.

We have studied reduction reactions of Se(VI), Pb(II), Cu(II), U(VI), Mo(VI), and Cr(VI). Upon reduction, all of these elements are expected to form sparingly soluble compounds. These reactions may be applied to clean waste- and groundwater.

Cytochrome c_3 was isolated from *Desulfomicrobium baculatum* [strain 9974] by the procedure of Moura et al. (1988), and the electrochemical potential of each of the four hemes was measured. Relative to the standard hydrogen electrode (SHE) the potentials are $E = -70$ mV for the heme with the lowest negative potential to $E = -350$ mV for the one with the highest negative potential and two potentials in between. The reason for selecting this cytochrome c_3 is that it has the highest negative potential compared with those purified from *Desulfovibrio* (*D. gigas*, *D. vulgaris*, and *D. desulfuricans*). Ma et al. (1998) attributed this highly negative potential to several effects, including high ruffling of the heme molecule.

A 0.1 M solution of sodium dithionite ($\text{Na}_2\text{S}_2\text{O}_4$) was prepared in a serum bottle and flushed with argon to remove oxygen. This solution was used to reduce cytochrome c_3 . Selenium was used in the form of Na_2SeO_4 , lead as $\text{Pb}(\text{NO}_3)_2$, copper as $\text{CuCl}_2 \cdot 2\text{H}_2\text{O}$, uranium as $\text{UO}_2(\text{NO}_3)_2 \cdot 10\text{H}_2\text{O}$, molybdenum as Li_2MoO_4 , and chromium as $\text{K}_2\text{Cr}_2\text{O}_7$. Stock solutions of these chemicals were prepared with concentrations between 1 and 18 mM by dissolving high-purity chemicals in a 30 mM sodium bicarbonate buffer solution ($\text{pH} = 7.3$). Only $\text{CuCl}_2 \cdot 2\text{H}_2\text{O}$ was dissolved in pure water to avoid precipitation of carbonates.

Each experiment began with the reduction of cytochrome c_3 and was conducted in a quartz cuvette placed in a Hewlett-Packard 8452 diode array UV-vis spectrometer: 10 μL of 0.1 M sodium dithionite solution were added to 1 mL of 10^{-5} M cytochrome c_3 solution. This yields a molar excess dithionite of at least 100. The spectrum of reduced cytochrome c_3 was recorded.

Then an aliquot of a stock solution of one of the metals was added sufficient to oxidize dithionite and cytochrome c_3 , and the spectrum of cytochrome c_3 was recorded again. Separate experiments were conducted for each metal. Enough precipitate (reduced metal species) was produced for analysis by transmission electron microscope. Blank experiments were conducted with de-ionized water alone and de-ionized water with nitrate to determine the effect of dissolved oxygen and nitrate on cytochrome c_3 oxidation.

At the end of a reduction/precipitation experiment, the cuvette was removed from the spectrometer and shaken. A few drops of the suspension were deposited onto a carbon-coated grid. Then, the grid was rinsed with de-ionized water to remove soluble salts. The grid was placed into a Jeol JEM-2010 transmission electron microscope (TEM), equipped with an Oxford Link ISIS EDS (energy-dispersive X-ray spectroscopy) system. Precipitates were analyzed for chemical composition, morphology, and crystal structure. Structural information was obtained using selected area electron diffraction (SAED). The microscope was operated at 200 keV.

We have shown for the first time that Se, Pb, Cu, and Mo are directly reduced by cytochrome c_3 . Our results suggest that cytochrome c_3 may be used as an efficient reducing agent in waste- and groundwater remediation. Even metal recovery may be considered. The redox reactions with cytochrome c_3 are very fast. Electrochemical reduction of cytochrome c_3 can avoid addition of chemicals to the system to be treated. Furthermore, we found that after several cycles of reduction-oxidation, cytochrome c_3 conserved its integrity and could be reused for metal reduction. Stability of cytochrome c_3 in aqueous solution, without significant loss of activity, is likely to be enhanced when immobilized.

Cytochrome c_3 can reduce metals in dissolved or in immobilized form, *i.e.* fixed on a substrate. Besides the couple hydrogenase- H_2 as electron provider for cytochrome c_3 , electrons for cytochrome c_3 reduction can be provided chemically by dithionite or electrochemically when immobilized on carbon electrodes. The gene for cytochrome c_3 from *D. vulgaris* has been cloned and expressed in the closely related *D. desulfuricans*, as well as the genetically distant *Rhodobacter sphaeroides*, suggesting the possibility of engineering an organism to overexpress cytochrome c_3 to enhance metal reduction. More recently, Aubert et al. (1998) showed that the gene encoding cytochrome c_7 from *D. acetoxidans* was expressed in *D. desulfuricans* that produces a relatively large quantity of cytochrome c_7 .

No measurements of final concentrations of the elements in solution were conducted. However, the precipitates observed and identified here are all known to be sparingly soluble. It is likely that solution concentrations are controlled by the solubility of the respective compounds after precipitation. Table 1 lists the precipitates. Their solubilities are compared with the United States Environmental Protection Agency's drinking water standards, indicating that the standards would be met in all cases. The stability of colloids (here: particle sizes of less than 100 nm) and their contribution to final concentrations in solution must be further investigated. Fig. 12 illustrates the nanoparticles

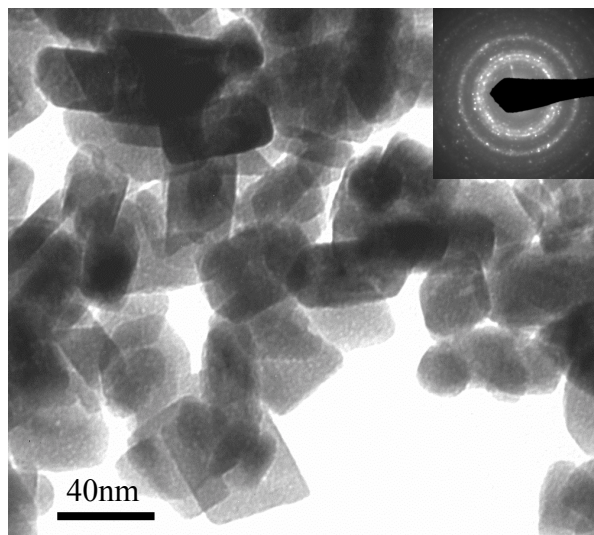


Fig. 12. Nanoparticle precipitate formed upon cytochrome c mediated reduction of a lead salt solution. Inset: EDS image.

of Pb^0 formed upon reduction by cytochrome c_3 .

Table 1. Phases precipitated by cytochrome c_3 , solubility in water at 25°C and EPA drinking water standards.

Solid phase	Solubility (M)	US EPA standard (M)*
Se^0 (red)	10^{-90} (Wagman et al., 1982)	$6.3 \cdot 10^{-7}$
Pb^0	10^{-12} (Ball & Nordstrom, 1998)	$2.4 \cdot 10^{-7}$
Cu^0	10^{-44} (Wolery, 1992)	$2 \cdot 10^{-5}$
UO_2	$1.9 \cdot 10^{-8}$ (Wolery, 1992)	$1.8 \cdot 10^{-7}$
MoO_2	10^{-57} (Lide, 1991)	10^{-6}
$\text{Cr}(\text{OH})_3$	10^{-60} (Wolery, 1992)	$9.6 \cdot 10^{-7}$

*(Federal Register, 1995)

We used cytochrome c_3 to reduce selenate (SeO_4^{2-}) to selenium (Se^0) with surprising results. Nanoparticles of Se^0 precipitated from an aqueous solution at room temperature, followed by spontaneous self-assembling into nanowires. Precipitation of Se^0 was indicated after one week when the solution turned red. The monoclinic modification of selenium is red. Nano-size particles with a spherical shape and an average diameter of 50 nm were found. SAED showed the precipitate to consist of a mixture of well-crystallized monoclinic and amorphous particles. Eventually, exposure of the crystallized particles to the electron beam led to loss of crystallinity. A week after nanoparticles started to form, the first nanowires appeared. The wires were about 60 nm in diameter and up to 1 μm long (Fig. 13). The d-spacings of this material were (in nm): 0.377, 0.325, 0.303, 0.283, 0.263, 0.220, 0.202, and 1.82, closely matching those of monoclinic selenium. EDS analysis showed that the wires consisted of selenium with some sulfur and traces of tellurium as impurities. Thicker wires may be due to attachment of nanoparticles to single strand wires (Fig. 14). Further aging of the precipitate led to formation of more wires with an average diameter below 100 nm and a length of a few micrometers. Se^0 particles and wires were stable in aqueous solution after ten weeks of storage. Electron beam irradiation caused the nanowires to become amorphous, but they did not disassemble. Thus, the catalytic function of cytochrome c_3 to accelerate certain reduction reactions may find further application in the field of nanomaterials synthesis.

Based on these results with the native cytochrome c_3 protein, it was thought that some porphyrins, *e.g.*, tin porphyrins, *without the surrounding protein matrix* might also be useful for mediating reduction reactions for metal salts. Using tin porphyrins to remove metals from solutions and, perhaps, to form metal nanoparticles is attractive

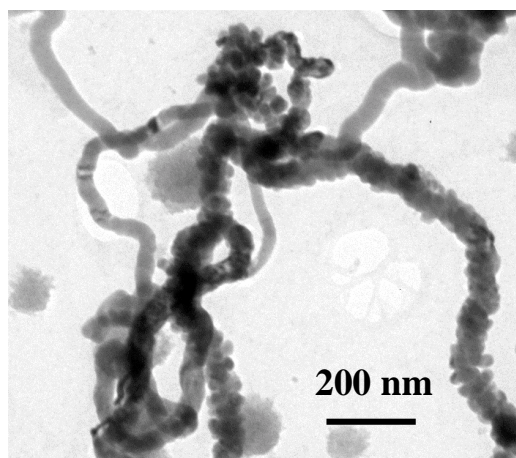


Fig. 13. TEM image of monoclinic (red) Se^0 nanowires formed by reduction of SeO_4^{2-} by cytochrome c_3 . Various forms of Se^0 particles and nanowires are shown in this view.

because it uses sun light as a source of energy to produce the required strongly reducing chemical species, replacing dithionite in the protein reactions.

Photoinduced redox reactions of a three-component system containing a photosensitizer, an electron donor, and an electron acceptor have been studied by several authors. Metallo-porphyrins are well studied photosensitizers for the reduction of various acceptor, usually methylviologen. For example, photoreduced tin porphyrins act as strong reductants in solution, in micelles, and at water-organic solvent interfaces, upon excitation by visible light and reduction by an electron donor such as a tertiary amine.

Shelnutt previously studied the ternary system comprised of Sn(IV) protoporphyrin IX (SnPP), triethanolamine (TEA), and methylviologen (MV^{2+}), where SnPP is the photosensitizer, TEA is the electron donor, and MV^{2+} is the electron acceptor. The photoinduced oxidation-reduction reaction is illustrated in Fig. 15. Irradiation of SnPP by visible light leads to excitation of the porphyrin to its lowest-lying triplet π - π state (SnPP*). Because the redox potential of the couple SnPP*/SnPP (+1.1 V) is higher than that of TEA/TEA_{ox} (+0.82 V), excited SnPP* accepts an electron from TEA resulting in the radical porphyrin anion (Fig. 15). The low redox potential of the SnPP^{•-}/SnPP couple (-0.66 V) allows the reduction of MV^{2+} to MV^+ (MV^{2+}/MV^+ ; -0.45 V). The quantum yield for the reaction is near 0.8.

The objective of this work was to investigate the possibility of reduction of a variety of metals by SnPP and light. Two types of metals were investigated: (1) U, Hg, Cu, and Pb which are common contaminants in wastewater and groundwater, and (2) Au, Ag, and Pt, which are precious metals. Thermodynamically, SnPP can reduce all these metal ions. Reduction reactions of the metals are listed in equations (1) to (7). For the first group of metals, their precipitation may be an interesting technique to remediate contaminated waters. For the second group, their concentration from aqueous solutions is a useful goal and is of interest in metal refining and materials processing.

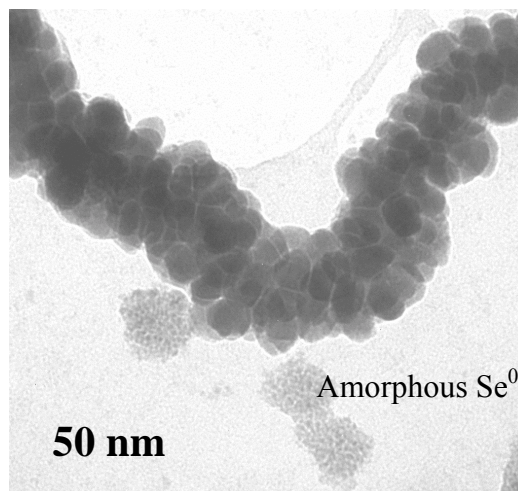
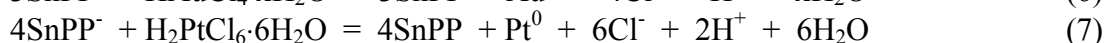
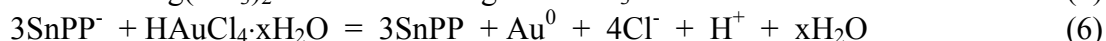
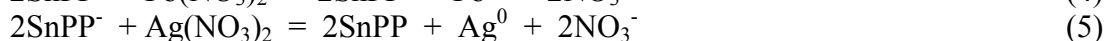
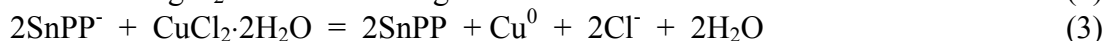


Fig. 14. TEM image showing nanoparticles in one of the "thick" (100 nm wide) Se^0 wires.

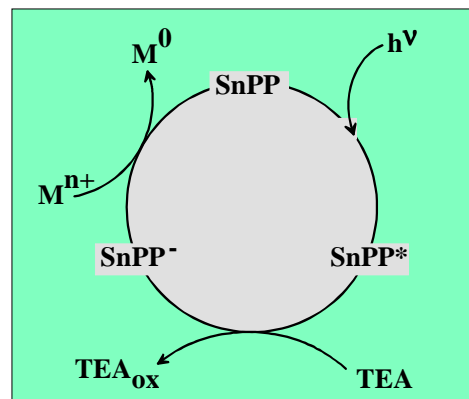


Fig. 15. The Sn-porphyrin photocycle used to reduce metal salts in aqueous solution. TEA = triethanolamine (or EDTA).

In the experiments with uranium, the appearance of a black precipitate was correlated with the decrease in the intensity of the yellow color of uranyl ion. The particles remained in suspension for several days. TEM results with uranium show U-rich particles; their electron diffraction pattern was also obtained. The particles are very small with an average diameter of 10 nm. The d -spacings (0.315, 0.274, 0.195, 0.164, 0.127 and 0.112 nm) of particles closely match those of cubic uraninite (UO_2). EDS measurements showed the particles consisted of U and O. In the experiment with Hg, a gray precipitate appeared after only a few minutes and deposited onto the bottom of the vial within the hour. The TEM images of the Hg-rich particles exhibit a spherical shape. The particles evaporated under the electron beam, a characteristic of liquid mercury. EDS measurements confirmed the presence of Hg^0 . It was

not possible to obtain SAED data. In the experiment with Cu, it took several days for a reddish coating to appear on the glass wall. TEM results with Cu show the morphology of the Cu-rich particles. These particles, with an average diameter of few microns, are aggregates of small particles (100 nm in diameter). These particles are pure Cu with traces of oxygen, which may indicate a slight oxidation of the surface of Cu. Attempts to obtain SAED data failed because the particles are too thick for the electron beam to penetrate. However, the red color of the precipitate, together with their composition, suggests the particles are Cu^0 . In the experiment with Pb, it took several days for a gray coating to appear on the glass wall. A TEM image of the Pb-rich precipitate along with their electron diffraction pattern show that the particles are well crystallized and measured d -spacings (0.288, 0.250, 0.176, 0.150, 0.124, 0.114 and 0.102 nm) match those of cubic Pb^0 . EDS measurements showed the particles consisted of Pb^0 .

The solubility of uraninite (2×10^{-8} M), Hg^0 (10^{-29} M), Cu^0 (10^{-44} M) and Pb^0 (10^{-60} M) in water at 25°C is very low. Therefore, their precipitation mediated by the tin protoporphyrin could be used to clean up contaminated waters. Following precipitation, these metal phases may be filtered for reuse or disposed of. Reductive precipitation of metals as a tool for water remediation is an active field of research and was recently proposed by several authors. Using SnPP for water remediation may be an attractive technique because it uses sun light as the source of energy to produce the strong reductant from an inexpensive and safe commonly-used emulsifier for vegetable oil, paraffin and waxes as the electron donor (triethanolamine).

Colloidal suspension of Ag-rich particles was obtained only a few minutes after the beginning of the experiment. A thin silver film also formed on the glass wall. The average size of these spherical particles was less than 20 nm in diameter. SAED data (0.280, 0.235, 0.200, 0.141, 0.119, 0.0985, 0.083 and 0.077 nm) match those of cubic Ag^0 , and EDS measurements showed the presence of Ag (Figure 6b). Experiments with Au showed the appearance of a golden suspension and correlated with the decrease in the intensity of the yellow color of gold chloride complex. Most particles are spherical with an average size of less than 20 nm in diameter. The measured d -spacings (0.220, 0.189, 0.132, 0.113, 0.109, 0.0967 and 0.085 nm) are similar to those of cubic Au^0 , and EDS analysis shows the presence of pure Au. In the

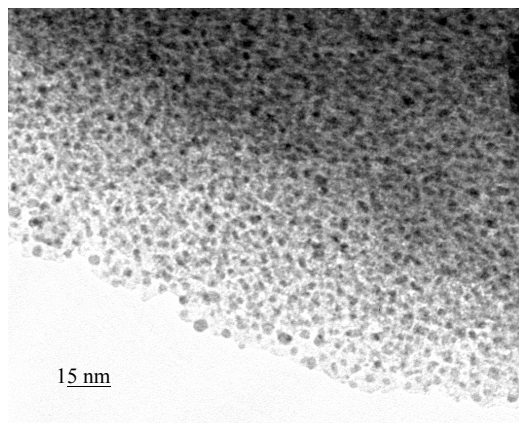


Fig. 16. TEM of a nanoporous silica hexagonal phase containing Ag^0 nanoparticles of 3-4 Å diameter. The particles are reductively precipitated from a $\text{Ag}(\text{NO}_3)_2$ aqueous solution containing triethanolamine by the embedded SnPP when exposed to sunlight.

experiment with Pt, a black precipitate appeared after few days and deposited onto the bottom of the vial. The particles consisted of rods with several microns in length and 300 nm in diameter. EDS measurements showed the particles consisted of Pt. We were not able to obtain SAED data because the particles were too thick for the electron beam to penetrate.

Precipitation of precious metals photosensitized by SnPP may be a practical way to extract and concentrate them from oxidizing waters. Furthermore, in the case of Au and Ag, formation of nanoparticles may find application in a variety of fields due to their optical properties. The present work is the first report of the formation of Au and Ag nanoparticles photomediated by a protoporphyrin at room temperature.

The tin porphyrin may be incorporated into mesoporous silicates to facilitate extraction from water streams. Figure 16 shows the TEM of a hexagonal nanophase of silica into which Sn protoporphyrin (SnPP) was incorporated at the time of sol-gel formation. The SnPP was included with the detergent (in at molar ratio of 1:670) that templates the nanostructured silica. After effusing with a metal salt solution containing triethanolamine and irradiating with sunlight, 3-4 nm particles are formed with the pores of the silicate. Higher concentrations of SnPP gave more closely spaced particles densely filling the mesopores. Precipitation of the metal particles within the silicate-porphyrin nanocomposite immobilizes and facilitates the subsequent removal of the metal particles from the waste stream.

Conclusions

Our program has brought to bear molecular simulation and computer-guided design and synthesis to develop a novel type of ionophore and catalytic and photocatalytic reductive precipitation technologies for solvent extraction treatments of heavy metal waste streams. The new solvent extraction processes enabled by the new ionophores address most of the metal extraction problems encountered at low- and high-level radioactive waste sites of interest to DOE. Specifically, the removal of heat emitters and long-lived radioisotopes from waste tanks, subsurface contaminants, heavy metals, and mixed waste treatment and disposal has been targeted. The work broadens the alternative technologies available for existent solvent-extraction treatments and enables new, more cost-effective extraction approaches. In addition, the new processes, especially the reductive precipitation methods, could potentially address some of the difficulties encountered in trace element separations.

We have shown that redox-sensitive metals, which are highly soluble in the oxidized state can be reduced and precipitated from aqueous solution using tin protoporphyrin and light in the presence of an electron donor. Hg^{2+} , Cu^{2+} and Pb^{2+} were reduced to the metallic state, and U^{6+} precipitated as oxide with very low solubility, suggesting that removal of these metals via reductive photoreduction and precipitation may be an innovative way for wastewater treatment. Ag^{2+} and Au^{3+} were reduced to the metallic state and precipitated as nanoparticles. Finally, using tin porphyrins and light for a variety of purposes involving reactions that require a low redox potential may be a good step toward energy conservation and environmentally benign processing.

Acknowledgements

Sandia is a multiprogram laboratory operated by Sandia Corporation, a Lockheed Martin Company, for the United States Department of Energy under Contract DE-AC04-94AL85000.

References

1. Richards, R. A., Hammons, K., Joe, M., and Miskelly, G. M. (1996) *Inorg. Chem.* 35, 1940-1944.
2. Shelnutt, J. A. (2000) in *The Porphyrin Handbook* (Kadish, K. M., Smith, K. M., and Guilard, R., Eds.) pp 167-223, Academic Press, New York.
3. Franco, R., Ma, J.-G., Lu, Y., Ferreira, G. C., and Shelnutt, J. A. (2000) *Biochemistry* 39, 2517-2529.
4. Franco, R., Ma, J. G., Lu, Y., Ferreira, G. C., and Shelnutt, J. A. (2000) *Biochemistry* 39, 2517-29.
5. Abdelouas, A., Gong, W. L., Lutze, W., Shelnutt, J. A., Franco, R., and Moura, I. (2000) *Chem. Mater.* V12, 1510-1512,4A.
6. Shelnutt, J. A. (2000) *J. Porphyrins Phthalocyanines* V4, 386-389.
7. Muzzi, C. M., Medforth, C. J., Smith, K. M., Jia, S. L., and Shelnutt, J. A. (2000) *Chem. Commun.*, 131-132.
8. Ma, J.-G., Vanderkooi, J. M., Zhang, J., Jia, S.-L., and Shelnutt, J. A. (1999) *Biochemistry* 38, 2787-2795.
9. Franco, R., Ma, J.-G., Lu, Y., Pereira, A., Tavares, P., Moura, I., Shelnutt, J. A., and Ferreira, G. C. (1999) *J. Inorg. Biochem.* 74, 130.
10. Shelnutt, J. A., Ma, J.-G., Zhang, J., Jia, S.-L., Lu, Y., and Vanderkooi, J. M. (1999) *J. Inorg. Biochem.* 74, 295.
11. Howes, B. D., Schiodt, C. B., Welinder, K. G., Marzocchi, M. P., Ma, J.-G., Zhang, J., Shelnutt, J. A., and Smulevich, G. (1999) *Biophys. J.* 77, 478-492.
12. Ma, J.-G., Zhang, J., Jia, S.-L., Lu, Y., Vanderkooi, J. M., and Shelnutt, J. A. (1999) *Biophys. J.* 76, A419.
13. Zhang, J., Celine, P., Jia, S. L., Ma, J. G., Shelnutt, J. A., and Marchon, J. C. (1999) *Biophys. J.* 76, A424 - A424.
14. Zhang, J., Ma, J. G., Jia, S. L., Borovkov, V. V., and Shelnutt, J. A. (1999) *Biophys. J.* 76, A424 - A424.
15. Howes, B. D., Schiodt, C. B., Welinder, K. G., Marzocchi, M. P., Ma, J. G., Zhang, J., Shelnutt, J. A., and Smulevich, G. (1999) *Biophys. J.* 77, 478-92.
16. Ma, J. G., Vanderkooi, J. M., Zhang, J., Jia, S. L., and Shelnutt, J. A. (1999) *Biochemistry* 38, 2787-95.
17. Nelson, N. Y., Medforth, C. J., Nurco, D. J., Jia, S. L., Shelnutt, J. A., and Smith, K. M. (1999) *Chem. Commun.*, 2071-2072.
18. Neal, T. J., Cheng, B. S., Ma, J. G., Shelnutt, J. A., Schulz, C. E., and Scheidt, W. R. (1999) *Inorg. Chim. Acta* V291, 49-59.
19. Muzzi, C. M., Medforth, C. J., Voss, L., Cancilla, M., Lebrilla, C., Ma, J. G., Shelnutt, J. A., and Smith, K. M. (1999) *Tetrahedron Lett.* V40, 6159-6162.
20. Howes, B. D., Schiodt, C. B., Welinder, K. G., Marzocchi, M. P., Ma, J. G., Zhang, J., Shelnutt, J. A., and Smulevich, G. (1999) *Biophys. J.* V77, 478-492.
21. Kadish, K. M., Van Caemelbecke, E., D'Souza, F., Lin, M., Nurco, D. J., Medforth, C. J., Forsyth, T. P., Krattinger, B., Smith, K. M., Fukuzumi, S., Nakanishi, I., and Shelnutt, J. A. (1999) *Inorg. Chem.* V38, 2188-2198.
22. Jia, S. L., Jentzen, W., Shang, M., Song, X. Z., Ma, J. G., Scheidt, W. R., and Shelnutt, J. A. (1998) *Inorg. Chem.* V37, 4402-4412.

23. Shelnut, J. A., Song, X. Z., Ma, J. G., Jia, S. L., Jentzen, W., and Medforth, C. J. (1998) *Chem. Soc. Rev.* 27, 31-41.
24. Song, X. Z., Jaquinod, L., Jentzen, W., Nurco, D. J., Jia, S. L., Khoury, R. G., Ma, J. G., Medforth, C. J., Smith, K. M., and Shelnut, J. A. (1998) *Inorg. Chem.* 37, 2009-2019.
25. Ma, J. G., Laberge, M., Song, X. Z., Jentzen, W., Jia, S. L., Zhang, J., Vanderkooi, J. M., and Shelnut, J. A. (1998) *Biochemistry* 37, 5118-5128.
26. Jentzen, W., Ma, J. G., and Shelnut, J. A. (1998) *Biophys. J.* 74, 753-63.
27. Drain, C. M., Gentemann, S., Roberts, J. A., Nelson, N. Y., Medforth, C. J., Jia, S. L., Simpson, M. C., Smith, K. M., Fajer, J., Shelnut, J. A., and Holten, D. (1998) *J. Am. Chem. Soc.* 120, 3781-3791.
28. Song, X. Z., Jentzen, W., Jaquinod, L., Khoury, R. G., Medforth, C. J., Jia, S. L., Ma, J. G., Smith, K. M., and Shelnut, J. A. (1998) *Inorg. Chem.* 37, 2117-2128.
29. Song, X. Z., Jia, S. L., Miura, M., Ma, J. G., and Shelnut, J. A. (1998) *J. Photochem. Photobiol. A-Chem.* 113, 233-241.
30. Jia, S. L., Zhang, J., Ema, T., Nelson, N. Y., Ma, J. G., Jentzen, W., Song, X. Z., Medforth, C. J., Smith, K. M., and Shelnut, J. A. (1998) *Biophys. J.* 74, A81.
31. Lemke, C., Shelnut, J. A., Quirke, J. M. E., Schweitzer-Stenner, R., and Dreybrodt, W. (1998) *Biophys. J.* 74, A83.
32. Ma, J. G., Zhang, J., Franco, R., Jia, S. L., and Shelnut, J. A. (1998) *Biophys. J.* 74, A133.
33. Ma, J.-G., Zhang, J., Franco, R., Jia, S.-L., Moura, I., Moura, J. J. G., Kroneck, P. M. H., and Shelnut, J. A. (1998) *Biochemistry* 37, 12431-12442.
34. Jia, S.-L., Jentzen, W., Shang, M., Song, X.-Z., Ma, J.-G., Scheidt, W. R., and Shelnut, J. A. (1998) *Inorg. Chem.* 37, 4407-4412.
35. Ma, J.-G., Laberge, M., Song, X.-Z., Jentzen, W., Jia, S.-L., Zhang, J., Vanderkooi, J. M., and Shelnut, J. A. (1998) *Biochemistry* 37, 5118-5128.
36. Shelnut, J. A., Song, X.-Z., Ma, J.-G., Jia, S.-L., Jentzen, W., and Medforth, C. J. (1998) *Chem. Soc. Rev.* 27, 31-41.
37. Ma, J. G., Zhang, J., Franco, R., Jia, S. L., Moura, I., Moura, J. J., Kroneck, P. M., and Shelnut, J. A. (1998) *Biochemistry* 37, 12431-42.
38. Lemke, C., Dreybrodt, W., Shelnut, J. A., Quirke, J. M. E., and SchweitzerStenner, R. (1998) *J. Raman Spectrosc.* V29, 945-953.
39. Ma, J. G., Zhang, J., Franco, R., Jia, S. L., Moura, I., Moura, J. J. G., Kroneck, P. M. H., and Shelnut, J. A. (1998) *Biochemistry* V37, 12431-12442.

UNLIMITED RELEASE

INITIAL DISTRIBUTION

	<u>Copies</u>	
MS1349	5	J. A. Shelnut
MS1349	1	J. E. Miller
MS1413	1	T. A. Michalske
MS1349	1	A. Hurd
MS1427	1	S. T. Picraux
MS0887	1	A. K. Hays
MS0161	1	Patent and Licensing Office, Org. 4331
MS0188	1	LDRD Office, Org. 4001
MS0612	1	Review and Approval Desk, Org. 4912 For DOE/OSTI
MS0899	5	Technical Library, Org. 4916
MS9018	1	Central Technical Files, Org. 8940-2